2014

Two-Dimensional Modeling of Thermoelectric Cells

Klaudio S. M. Oliveira
UFPR, Brazil, klaudio@uol.com.br

Rodrigo P. Cardoso
UFPR, Brazil, rodrigo.perito@ufpr.br

Christian J. L. Hermes
UFPR, Brazil, chermes@ufpr.br

Two-Dimensional Modeling of Thermoelectric Cells

Klaudio S. M. OLIVEIRA, Rodrigo P. CARDOSO*, Christian J. L. HERMES

Laboratory of Thermodynamics and Thermophysics, Department of Mechanical Engineering
Federal University of Paraná, 81531990 Curitiba-PR, Brazil
* Corresponding author: rodrigo.perito@ufpr.br

ABSTRACT

The present paper is aimed at putting forward a two-dimensional model for thermoelectric cells. The energy conservation equation was formulated in order to account for the Fourier, the Thomson and the Joule effects on the temperature distribution. The electric field was also solved to come out with the current and voltage distributions. The governing equations were discretized by means of the finite-volume method, whereas the TDMA algorithm was adopted for solving the sets of linear equations. An explicit iterative solution scheme was employed to address the temperature influence on the Seebeck coefficient. The model results were compared with experimental data, when a satisfactory agreement was achieved for both cooling capacity and COP, with errors within a ±10% band. In addition, the model was employed to assess the effects of the thermoelectric properties and the couple geometry on the thermodynamic performance of the thermoelectric cell.

1. INTRODUCTION

In the past decades, solid-state cooling technologies have come onto particular market niches, especially the applications related to portable cooling (Hermes and Barbosa, 2012). The most significant advances have been achieved in the realm of the thermoelectric cooling, in which an electric current produces a temperature difference in a pair of dissimilar semiconductor materials. A typical thermoelectric module is manufactured with two thin ceramic wafers and an array of p- and n-type blocks of doped semiconductor material sandwiched between them. A pair of p- and n-type blocks connected electrically in series and thermally in parallel make up a thermoelectric couple.

Several studies have been conducted both theoretically and numerically to assess the thermodynamic performance of thermoelectric cells. Some influencing works are summarized in Tab. 1. The literature review points out that most models are one-dimensional, being not able to evaluate the influence of the couple geometry on its performance. In addition, the literature analysis also reveals that the few available multidimensional (2D/3D) models are often developed aided by commercial packages, which not only restrict the access to the mathematical formulation, but also to the numeric scheme. At last, most models do not account for the heat transfer in the air cavity, which also might affect the system performance. The present paper is therefore aimed at advancing a two-dimensional model, in the realm of non-equilibrium thermodynamics, which is able to evaluate the sensitivity of the thermophysical properties and the cell geometry on its thermodynamic performance.

Table 1: Summary of the recent literature on performance assessment of thermoelectric cells

Author	Year	Approach	Thomson effect	Cavity convection	Cavity radiation	Physical Domain	Properties as f=f(T)
Huang et al.	2005	Analytical	Yes	Yes	Yes	1D	No
Pramanickand Dass.	2006	Analytical	Yes	No	No	1D	No
Lee and Kim	2006	Numerical	No	No	No	1D	No
Yamashita	2009	Analytical-Experimental	Yes	No	No	1D	Yes
Chen et al.	2011	Numerical	Yes	Yes	Yes	3D	No
Meng et al.	2011	Numerical	Yes	Yes	Yes	1D	Yes
Du and Wen	2011	Numerical-Experimental	Yes	No	No	1D	Seebeck only
Chen et al.	2012	Numerical	Yes	No	No	3D	Seebeck only
Pérez-Aparicio et al.	2012	Numerical	Yes	Yes	Yes	3D	Yes

2. MATHEMATICAL FORMULATION

A thermoelectric cell is comprised of several pairs of p and n semiconductors connected electrically in series and thermally in parallel, and separated from each other by a cavity filled with air. The physical model is restricted to a thermoelectric pair, as illustrated in Fig. 1, which in turn is subdivided into ten domains, as summarized in Tab. 2. The dimensions in Tab. 2 refer to the thermoelectric device (Tellurex, 2007), which has been taken as reference for the present study.

The mathematical model is based on the following key assumptions: (i) steady-state two-dimensional model, (ii) the thermophysical properties of each material are function of the temperature only, (iii) the internal contact resistances (both thermal and electric) are negligible, (iv) both n and p elements have the same Seebeck coefficient, but with different signs, and (v) the heat transfer by both advection and radiation are disregarded, so that Nu=1 (pure heat conduction) in the cavity. Hence, a local energy balance yields,

$$\vec{\nabla}\cdot\vec{q} = \dot{q} \tag{1}$$

where $\dot{q}$ is the rate of heat generation, and the heat flux, $\vec{q}$, is calculated from the following relation obtained from the irreversible thermodynamics (Reynolds, 1968):

$$\vec{q} = -k\vec{\nabla}T + \alpha T\vec{j} \tag{2}$$

where the first term on the right-hand side stands for the heat conduction (referred hereafter as Fourier effect), where k is the thermal conductivity, and the second term is associated with the Seebeck effect, being α the Seebeck coefficient. The divergent of eq. (2) yields,

$$\vec{\nabla}\cdot\vec{q} = -\vec{\nabla}\cdot\left(k\vec{\nabla}T\right) + \vec{j}\cdot\vec{\nabla}(\alpha T) + \alpha T\left(\vec{\nabla}\cdot\vec{j}\right) \tag{3}$$

where $\vec{\nabla}\cdot\vec{j} = 0$ at steady-state conditions to ensure the continuity of the electron flux. In addition, the definition of electric field yields,

$$-\vec{\nabla}V = \rho\vec{j} + \alpha\vec{\nabla}T \tag{4}$$

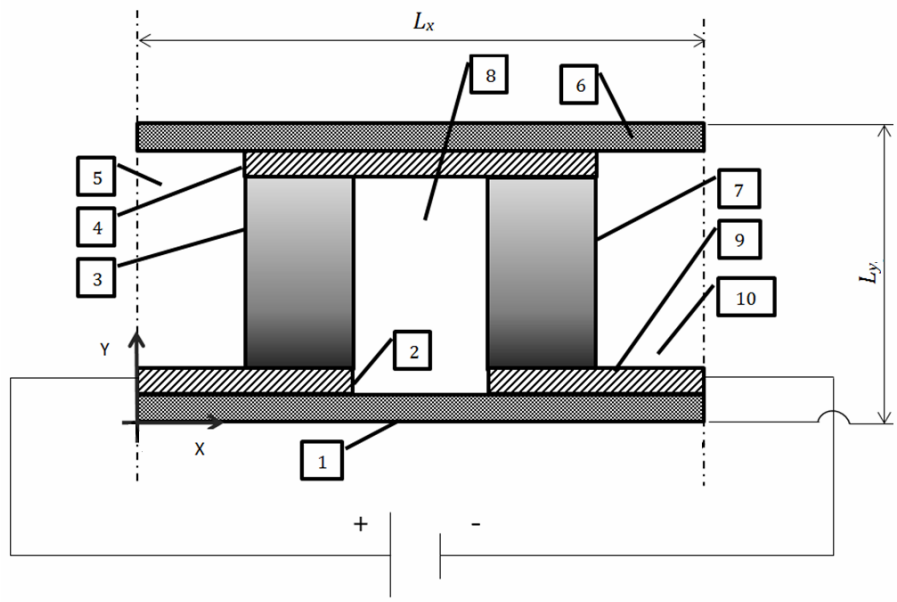

Figure 1: Schematic representation of the physical model

Table 2: Summary of the physical domains

Subdomain	Description	Material	Dimensions [mm]
1 & 6	Bottom (1) and top (6) electric insulators	Al_2O_3	4.8 x 0.62
2 & 9	Left (2) and right (9) electric conductors at the bottom	Cu	1.9 x 0.41
3 & 7	n-type (3) and p-type (7) semiconductors	Bi_2Te_3	1.4 x 1.14
4	Electric conductor at the top	Cu	1.9 x 0.41
5 & 10	Left (5) and right (10) side air cavities	Air	0.5 x 1.55
8	Central air cavity	Air	1.0 x 1.55

Therefore, the rate of heat generation $\dot{q}$ is calculated as follows:

$$\dot{q} = \vec{j} \cdot \left(-\vec{\nabla} V\right) = \rho\left(\vec{j} \cdot \vec{j}\right) + \alpha \vec{j} \cdot \vec{\nabla} T \tag{5}$$

where the first term on the right-hand side stands for the Joule heating, whereas the second term is regarded with the work produced by the electric current against the Seebeck effect. Invoking the 2nd thermoelectric relation,

$$\tau dT = T d\alpha \tag{6}$$

and replacing eqs. (3) and (5) into eq. (1), the following equation for the temperature distribution in a thermoelectric material can be derived,

$$\vec{\nabla} \cdot \left(k \vec{\nabla} T\right) - \tau \vec{j} \cdot \vec{\nabla} T + \rho\left(\vec{j} \cdot \vec{j}\right) = 0 \tag{7}$$

where the first term refers to the Fourier conduction, the second one to the Thomson (thermoelectric) effect, and the third to the Joule heating. Writing eq. (4) for the electric current, and recalling that $\vec{\nabla} \cdot \vec{j} = 0$ at steady-state conditions, one can derive the following expression for the voltage distribution along the domain,

$$\vec{\nabla} \cdot \left(\gamma \vec{\nabla} V\right) + \vec{\nabla} \cdot \left(\gamma \alpha \vec{\nabla} T\right) = 0 \tag{8}$$

where $\gamma = \rho^{-1}$ is the electrical conductivity. The first term stands for the electric conduction, whereas the second one refers to the distortion on the electric field induced by the thermoelectric effect. Equation (7) and (8) rule the thermoelectric phenomena, being both expressed for 2-D Cartesian domain as follows:

$$\frac{\partial}{\partial x}\left(k \frac{\partial T}{\partial x}\right) + \frac{\partial}{\partial y}\left(k \frac{\partial T}{\partial y}\right) - \tau\left(j_x \frac{\partial T}{\partial x} + j_y \frac{\partial T}{\partial y}\right) + \rho\left(j_x^2 + j_y^2\right) = 0 \tag{9}$$

$$\frac{\partial}{\partial x}\left(\gamma \frac{\partial V}{\partial x}\right) + \frac{\partial}{\partial y}\left(\gamma \frac{\partial V}{\partial y}\right) + \frac{\partial}{\partial x}\left(\gamma\alpha \frac{\partial T}{\partial x}\right) + \frac{\partial}{\partial y}\left(\gamma\alpha \frac{\partial T}{\partial y}\right) = 0 \tag{10}$$

where j_x and j_y are the x and y components of the electric current density, respectively, in [A/m^2]. Equations (9) and (10) require two boundary conditions each. For the latter, prescribed inlet (V_{in}) and outlet (V_{out}) voltages were adopted. In addition, bearing in mind that there is no electron flux through subdomains 1 and 6, dV/dy=0 boundary conditions have also been adopted. In case of eq. (9), prescribed temperatures were used for both hot (T_h) and cold (T_c=T_h-ΔT) ends. Zero heat flux boundary conditions (dT/dx=0) were also employed for the cell symmetry. Figure 2 depicts the conditions used for each boundary of the physical domain. The thermophysical properties of the Bi_2Te_3-elements were calculated from 2nd-order polynomial fits obtained from data provided by Rowe (1995),

$$\rho = 2.3935 \cdot 10^{-11} T^2 + 2.9771 \cdot 10^{-8} T - 8.959 \cdot 10^{7} \tag{11}$$

$$k = 3.682 \cdot 10^{-5} T^2 - 2.372 \cdot 10^{-2} T + 5.388 \tag{12}$$

$$\alpha = -8.5952 \cdot 10^{-10} T^2 + 8.0546 \cdot 10^{-7} T + 4.329 \cdot 10^{-5} \tag{13}$$

where T is in [K], ρ in [Vm/A], k in [W/mK], and α in [V/K]. The Thomson coefficient, τ, was calculated from eqs. (6) and (13). Both the air and the Al_2O_3-elements were assumed to be perfect electric insulators, with thermal conductivities (at 300 K) of 30 and 0.026 W/mK, respectively. For the copper, a thermal conductivity of 400 W/mK and an electrical resistivity of $1.687 \cdot 10^{-8}$ Vm/A have been adopted. The heat transfer inside the air cavity was modeled assuming a unitary Nusselt number, so the effects of free convection and radiation were neglected.

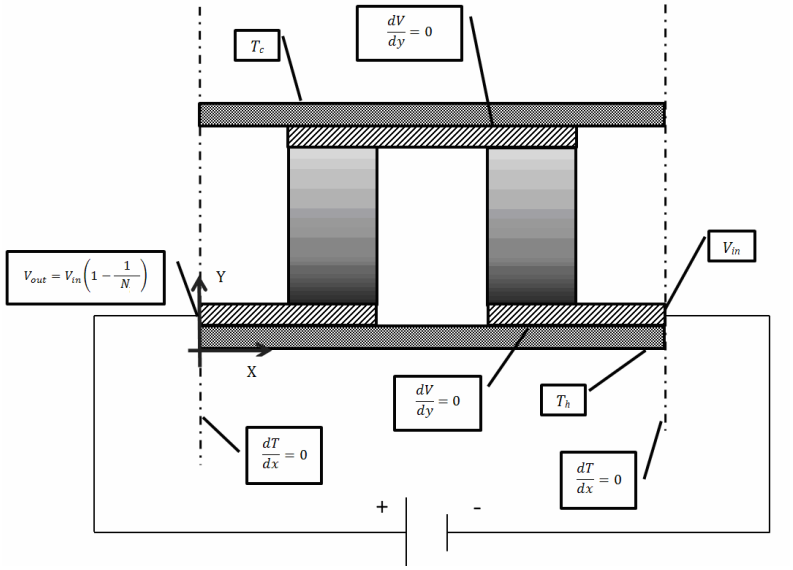

Figure 2: Schematic representation of the boundary conditions

3. NUMERICAL SCHEME

Because of the non-linearities, eqs. (9) and (10) have to be solved iteratively to come out with the temperature and voltage distributions along the domain. A computational code was written based on the so-called finite-volume method (Patankar, 1980). The method consists of dividing the physical domain into non-overlaping control volumes in which the mass, momentum and energy quantities are conserved. The centroid of each control volume, as illustrated in Fig. 3.a, corresponds to an integration cell of the discretized domain. The properties (T, V) are evaluated at the centroids, whereas the fluxes (q, j) are evaluated at the control surfaces. A non-uniform Cartesian mesh was generated by means of the equation introduced by Wood (1996). Mesh independent solutions have been found for computational grids with 3000+ control volumes. A snapshot of a computational domain with 3120 control volumes is depicted in Fig. 3.b.

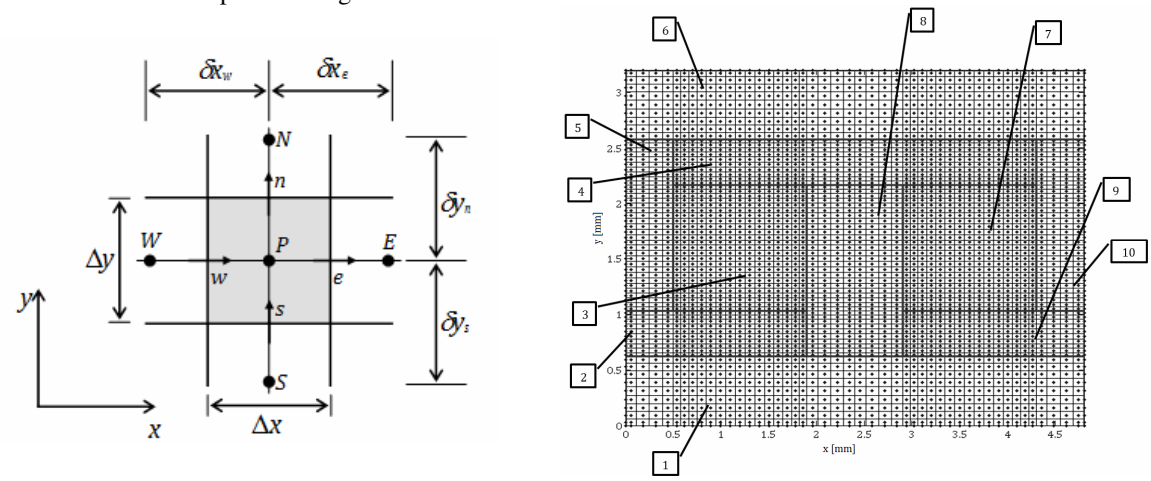

(a) (b)

Figure 3: Computational mesh: (a) typical control volume, (b) non-uniform grid with 3120 control volumes

Equations (9) and (10) were discretized using a 2nd order central-differencing scheme. The non-linear terms have been incorporated into the source term. The resulting algebraic equations for temperature and voltage are as follows:

$$A_P^T T_P = A_e^T T_E + A_w^T T_W + A_n^T T_N + A_s^T T_s + B^T$$

$$\begin{cases} A_e^T = k_e \Delta y / \delta x_e \\ A_w^T = k_w \Delta y / \delta x_w \\ A_n^T = k_n \Delta x / \delta y_n \\ A_s^T = k_s \Delta x / \delta y_s \\ A_P^T = A_e^T + A_w^T + A_n^T + A_s^T \\ B^T = \rho_P \left(j_x^2 + j_y^2 \right) \Delta x \Delta y - \tau_P \left(j_x \left(T_e^* - T_w^* \right) \Delta y + j_y \left(T_n^* - T_s^* \right) \Delta x \right) \end{cases} \quad (14)$$

$$A_P^V V_P = A_e^V V_E + A_w^V V_W + A_n^V V_N + A_s^V V_s + B^V$$

$$\begin{cases} A_e^V = \gamma_e \Delta y / \delta x_e \\ A_w^V = \gamma_w \Delta y / \delta x_w \\ A_n^V = \gamma_n \Delta x / \delta y_n \\ A_s^V = \gamma_s \Delta x / \delta y_s \\ A_P^V = A_e^V + A_w^V + A_n^V + A_s^V \\ B^V = \alpha_e A_e^V T_E^* + \alpha_w A_w^V T_W^* + \alpha_n A_n^V T_N^* + \alpha_s A_s^V T_S^* - \left(\alpha_e A_e^V + \alpha_w A_w^V + \alpha_n A_n^V + \alpha_s A_s^V \right) T_P^* \end{cases} \quad (15)$$

where the superscript asterisk stands for the property available from the previous iteration. The sets of linear equations have been solved iteratively through the TDMA algorithm. The properties at the interfaces between different materials have been calculated in order to guarantee the continuity of the electron and heat fluxes. More detailed information on the numerical scheme can be found in Oliveira (2014).

4. MODEL VALIDATION

The code predictions were validated against experimental data obtained from the manufacturer of a particular thermoelectric module. All simulations were carried out for T_h=323 K, but varying the ΔT between the hot and the cold ends from 0 to 60 K, and the ΔV applied to the whole thermoelectric module from 11 to 16 V. Figure 4 shows a comparison between the calculated and measured electric current, where one can see the maximum difference achieved (for ΔT=0 K and ΔV=16 V) was below the 10% threshold. In all cases, one can see the model is able to follow the experimental trends closely.

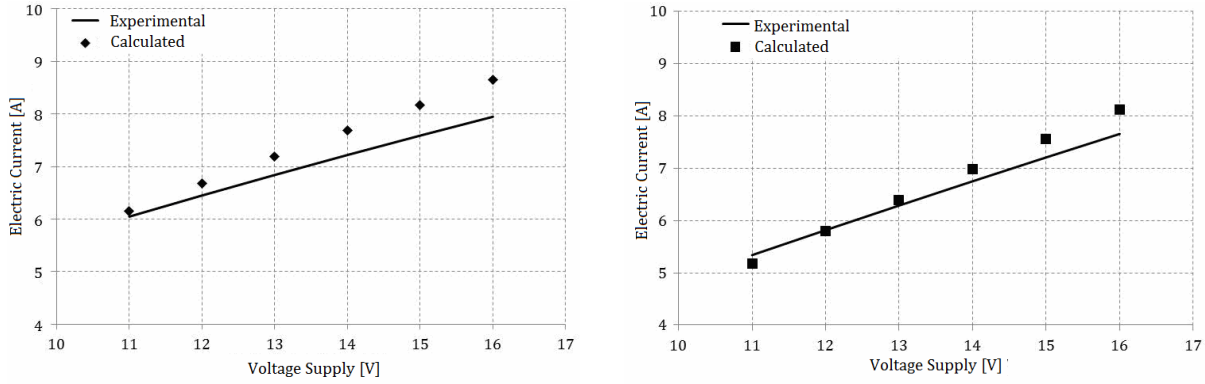

(a) (b)

Figure 4: Comparison between calculated and experimental electric current: (a) ΔT=0 K, (b) ΔT=60 K

Additional validation parameters are the cooling capacity $\dot{Q}_c$ and the COP, calculated respectively as follows:

$$\dot{Q}_c = NL_z \sum_{i=1}^{n} \left(k \frac{T_m - T_c}{\delta y_m} \Delta x \right)_i \tag{16}$$

$$COP = \frac{\dot{Q}_c}{\dot{Q}_h - \dot{Q}_c} \tag{17}$$

where $\dot{Q}_h$ is the heat released at the hot end, calculated as follows:

$$\dot{Q}_h = NL_z \sum_{i=1}^{n} \left(k \frac{T_h - T_l}{\delta y_l} \Delta x \right)_i \tag{18}$$

where L_z is the cell dimension in the z direction (perpendicular to the paper sheet), N is the number of thermoelectric pairs in the cell, and n and m are the number of control volumes in the x and y directions, respectively. Figure 5 shows the calculated and the experimental cooling capacities agreed to with errors within the 10% threshold. The higher difference is observed for low voltages and ΔT=0 K. A similar behavior is observed in Fig. 6 for the COP. In all cases, the experimental trends are well reproduced by the model.

Figure 7 explores the temperature distributions obtained for four different cases: (a) no thermoelectric effect (Joule heating only) and ΔT=0 K, (b) thermoelectric effect and ΔT=0 K, (c) thermoelectric effect and ΔT=30 K, and (d) thermoelectric effect and ΔT=60 K. In all cases, ΔV=16 V. The temperature profiles along the A-A cut (at x=1.1 mm) are also depicted in Fig. 7. For case (a), where no thermoelectric effect takes place, one can see that the Joule heating is symmetrically dissipated by Fourier conduction in such a way the maximum temperature takes place at the center of the thermoelectric elements. This is so as ΔT=0 K. In cases the thermoelectric effect is on, the locus of the maximum temperature migrates from the center to the bottom inasmuch the ΔT increases.

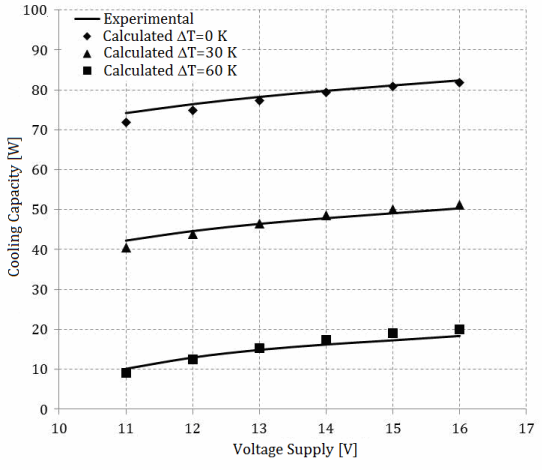

Figure 5: Comparison between calculated and experimental cooling capacity

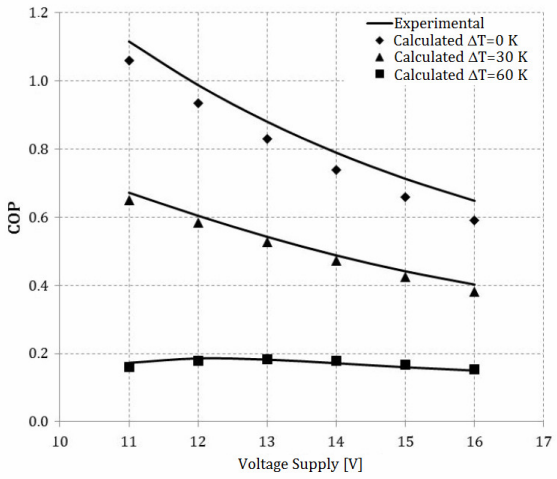

Figure 6: Comparison between calculated and experimental COP

5. SENSITIVITY ANALYSIS

5.1 Sensitivity to Thermophysical Properties

The sensitivity analysis was carried out considering as response variables the cooling capacity and the COP, whereas the thermophysical properties (i.e. thermal conductivity, Seebeck coefficient, and electric conductivity) were taken as independent parameters.

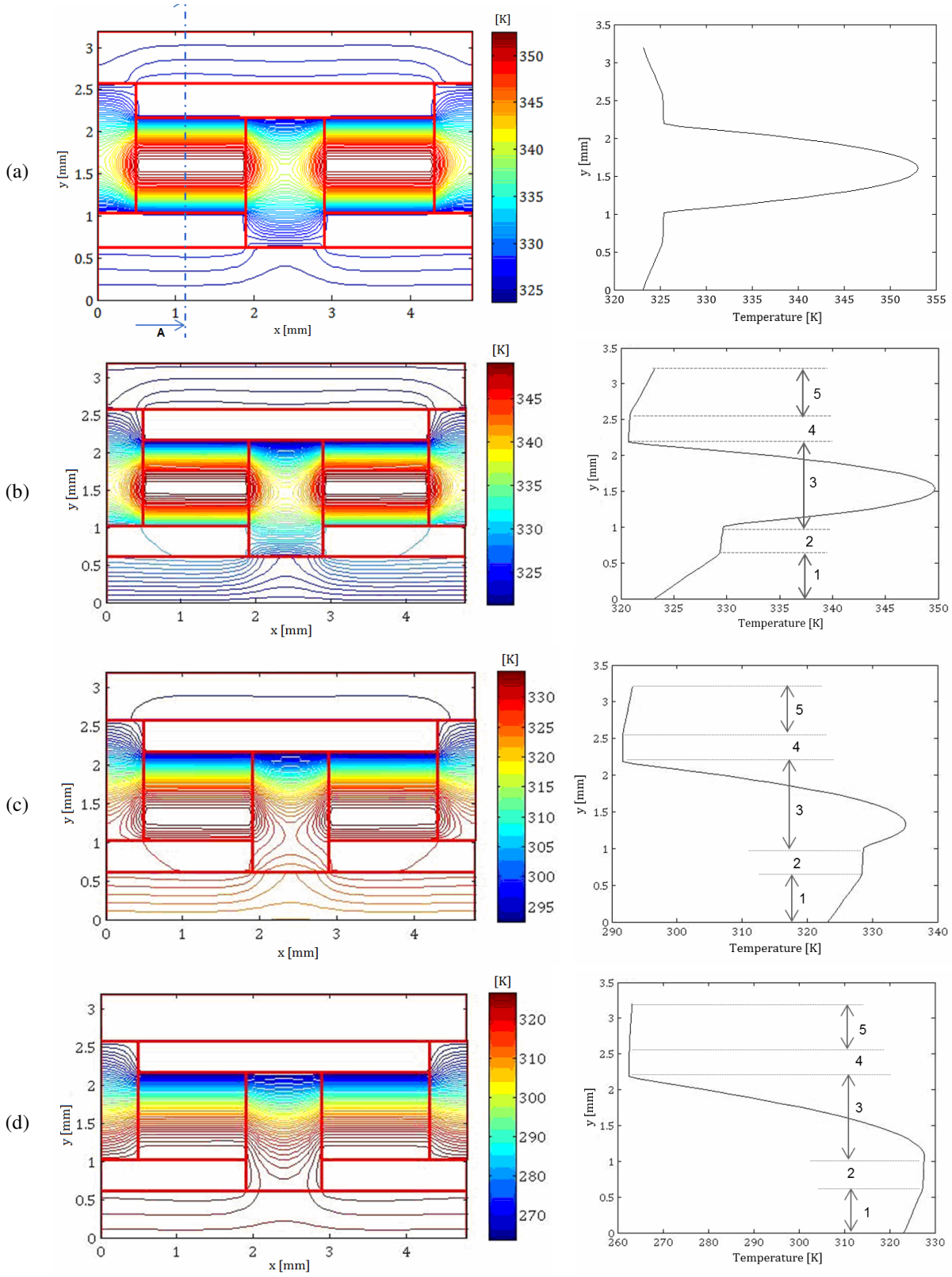

Figure 7: Temperature distribution along the domain for ΔV=16 V and different ΔT

A 2-level, 3-factor factorial design was then planned totalizing 2^3=8 runs. The levels were set as ±5% spans taking the figures provided by eqs. (11) to (13) as reference. The simulation runs were carried out for ΔT=0 K and ΔV=16 V. The regression model adopted in this work is as follows:

$$\hat{\Psi} = \lambda_0 + \lambda_1\hat{k} + \lambda_2\hat{\alpha} + \lambda_3\hat{\gamma} + \lambda_4\hat{k}\hat{\alpha} + \lambda_5\hat{k}\hat{\gamma} + \lambda_6\hat{\alpha}\hat{\gamma} + \lambda_7\hat{k}\hat{\alpha}\hat{\gamma} \tag{19}$$

where γ=1/ρ is the electric conductivity, $\hat{\Psi}$ is the dimensionless response variable, λ are the coefficients calculated from the least-squares method, and $\hat{\varphi}$ are the dimensionless values of φ, calculated from:

$$\hat{\varphi} = 2(\varphi - \varphi_{min})/(\varphi_{max} - \varphi_{min}) - 1 \tag{20}$$

Figure 8 shows the cooling capacity is mainly affected by the electric conductivity and the Seebeck coefficient, and marginally affected by the thermal conductivity, which play a negative role on the cooling capacity. The higher-order interactions have not played any material effects on the cooling capacity. Figure 8 also shows the effects of the thermophysical properties over the COP, where one can see the Seebeck coefficient plays a dominant role, followed by the thermal and electric conductivities, which played a marginal role. These treds are confirmed by the definition of the figure-of-merit of the thermoelectric material, Z= $\alpha^2\gamma$/k, which is straightforwardly related to the COP.

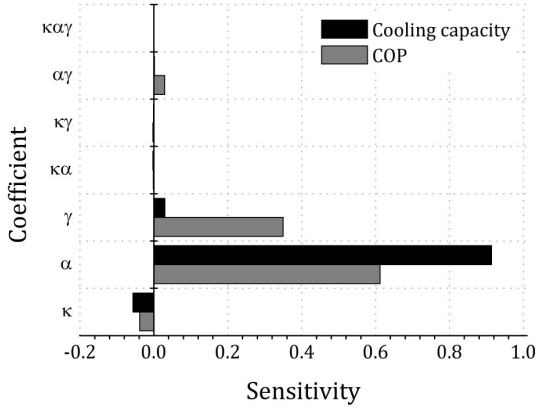

Figure 8: Results of the sensitivity analysis: cooling capacity and COP

5.2 Sensitivity to Aspect Ratio

To assess the influence of the geometry, the aspect ratio was varied by increasing the height of the thermoelectric cell, L_y, in two fashions: (a) constrained base area (i.e. fixed L_x, see Fig. 9), and (b) constrained volume of thermoelectric material (see Fig. 10). In all cases, ΔT=0 K and the voltage was varied from 14 to 20 V. Figure 11 shows the COP is weakly affected by L_y. Indeed, a slight increase can be observed. This is so as the cooling capacity depletes inasmuch the electric current decreases, which diminishes the power consumption at the same rate. As the COP is the ratio between the cooling capacity and the power consumption, one can expect the COP figure is not significantly changed from one case to the other.

Figure 9: Samples of geometries analyzed in case of constrained base area: (a) aspect ratio ½, (b) aspect ratio 2

(a) (b)

Figure 10: Samples of geometries analyzed in case of constrained volume: (a) aspect ratio ½, (b) aspect ratio 2

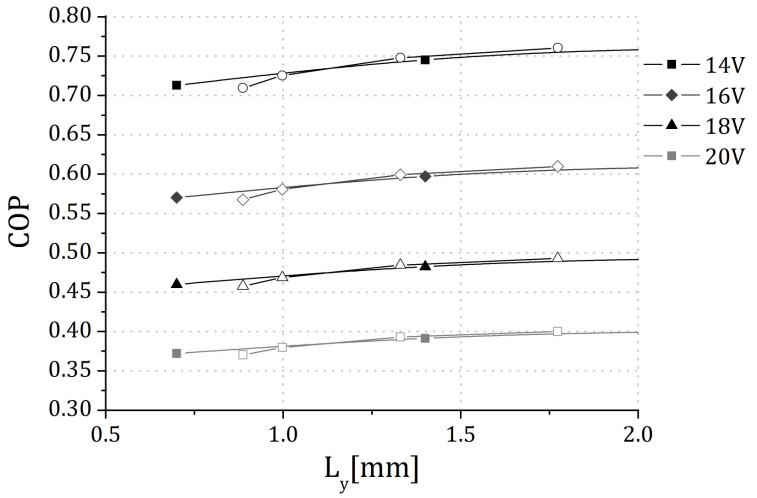

Figure 11: Influence of the aspect ratio on the COP in case of constrained area (solid bullets) and constrained volume (open bullets)

6. CONCLUDING REMARKS

A first-principles two-dimensional steady-state model was put forward to evaluate the thermodynamic performance of thermoelectric cells in the realm of the non-equilibrium (irreversible) thermodynamics. The model takes into account the Fourier conduction, the Joule heating, and the Thomson effect, being able to predict the cooling capacity, the power consumption, and the COP in case of prescribed voltage supply and prescribed temperatures at the hot and cold ends. The governing equations were discretized by means of the finite-volume method using a central-differencing scheme. The non-linearities typical of the thermoelectric phenomena were embedded into the source term, and the resulting sets of algebraic equations were solved iteratively by the TDMA algorithm.

The tailor-made model was coded in-house and its predictions for electric current, cooling capacity and COP were compared against experimental data obtained from the manufacturer of a particular thermoelectric cell. It was observed the numerical predictions and experimental data not only agreed to within 10% thresholds, but also the model is able to follow the experimental trends very closely.

The influence of the thermophysical properties on the response variables (cooling capacity and COP) was assessed by means of a 2^3 factorial design, which has pointed out that the Seebeck coefficient and the thermal conductivity play major roles on the cooling capacity, whereas the COP is more sensible to the Seebeck coefficient. The influence of the geometry was also assessed by varying the aspect ratio according to two different ways: constrained base area and constrained volume. It was observed that both the cooling capacity and the power consumption vary at the same rates, in such a way the COP, which relates the cooling capacity and the power consumption, has showed a similar behavior for constrained base area and constrained volume of thermoelectric material.

NOMENCLATURE

Roman

COP	coefficient of performance [W/W]
j	electric current density [A m^{-2}]
k	thermal conductivity [W $m^{-1}K^{-1}$]
L_x	width [m]
L_y	height [m]
L_z	length [m]
m	number of integrating cells (y-direction)
n	number of integrating cells (x-direction)
N	number of thermoelectric pairs in the cell
$\dot{q}$	heat generation [W m^{-3}]
q	heat flux [W m^{-2}]
$\dot{Q}$	heat transfer rate [W]
T	temperature [K]
V	voltage [V]
Z	figure-of-merit [K^{-1}]

Greek

α	Seebeck coefficient [V K^{-1}]
γ	electrical conductivity [V^{-1} m^{-1} A]
φ	generic variable
ρ	electrical resistivity [V m A^{-1}]
τ	Thomson coefficient [V K^{-1}]

Subscripts

c	cold end
e, w, n, s	control surfaces
P, E, W, N, S	control volumes
h	hot end

REFERENCES

Chen M, Rosendahl LA, Condra T, A three-dimensional numerical model of thermoelectric generators in fluid power systems, *Int. J. Heat Mass Transfer* 54 (2011) 345–355

Chen W, Liao C, Hung C, A numerical study on the performance of miniature thermoelectric cooler affected by Thomson effect, *Applied Energy* 89 (2012) 464-473

Reynolds WC, 1968, *Thermodynamics*, McGraw-Hill, New York, USA

Du C, Wen C, Experimental investigation and numerical analysis for one-stage thermoelectric cooler considering Thomson effect, *Int. J. Heat Mass Transfer* 54 (2011) 4875-4884

Hermes CJL, Barbosa JR, Thermodynamic comparison of Peltier, Stirling, and vapor compression portable coolers, Applied Energy, *Applied Energy* 91 (2012) 51–58

Huang M, Yen R, Wang A, The influence of the Thomson effect on the performance of a thermoelectric cooler, *Int. J. Heat Mass Transfer* 48 (2005) 413-418

Lee KH, Kim OJ, Analysis on the cooling performance of the thermoelectric micro-cooler, *Int. J. Heat Mass Transfer* 50 (2006) 1892-1992

Meng F, Chen L, Sun F, A numerical model and comparative investigation of a thermoelectric generator with multi-irreversibilities, *Energy* 36 (2011) 3513-3522

Oliveira KMS, 2014, *Numerical Assessment of the Thermodynamic Behavior of Thermoelectric Cells*, M.Eng. thesis, Federal University of Paraná, Curitiba-PR, Brazil, 140p. (in Portuguese)

Patankar SV, 1980, *Numerical Heat Transfer and Fluid Flow*, Hemisphere Publishing Co., New York, USA

Pérez-Aparicio JL, Palma R, Taylor RL, Finite element analysis and material sensitivity of Peltier thermoelectric cells coolers, *Int. J. Heat Mass Transfer* 55 (2012) 1363-1374

Pramanick AK, Das PK, Constructal design of a thermoelectric device, *Int. J. Heat Mass Transfer* 49 (2006) 1420-1429

Rowe D, 1995, *CRC Handbook of Thermoelectrics*, CRC Press, Boca Raton-FL, USA

Tellurex, 2007, *Module Specification Z-max C1-1.4-127-1.14*, Traverse City-MI, USA

Wood WA, 1996, *Multigrid Approach to Incompressible Viscous Cavity Flow*, Technical Memorandum, NASA Langley Research Center, Hampton-VA, USA

Yamashita O, Effect of linear and non-linear components in the temperature dependences of thermoelectric properties on the cooling performance, *Applied Energy* 86 (2009) 1746-1756

ACKNOWLEDGEMENTS

Financial support from the Brazilian funding agencies CAPES and CNPq is duly acknowledged.